iScience

CellPress
OPEN ACCESS

Article

$NaNbO_3$/ZnO piezocatalyst for non-destructive tooth cleaning and antibacterial activity

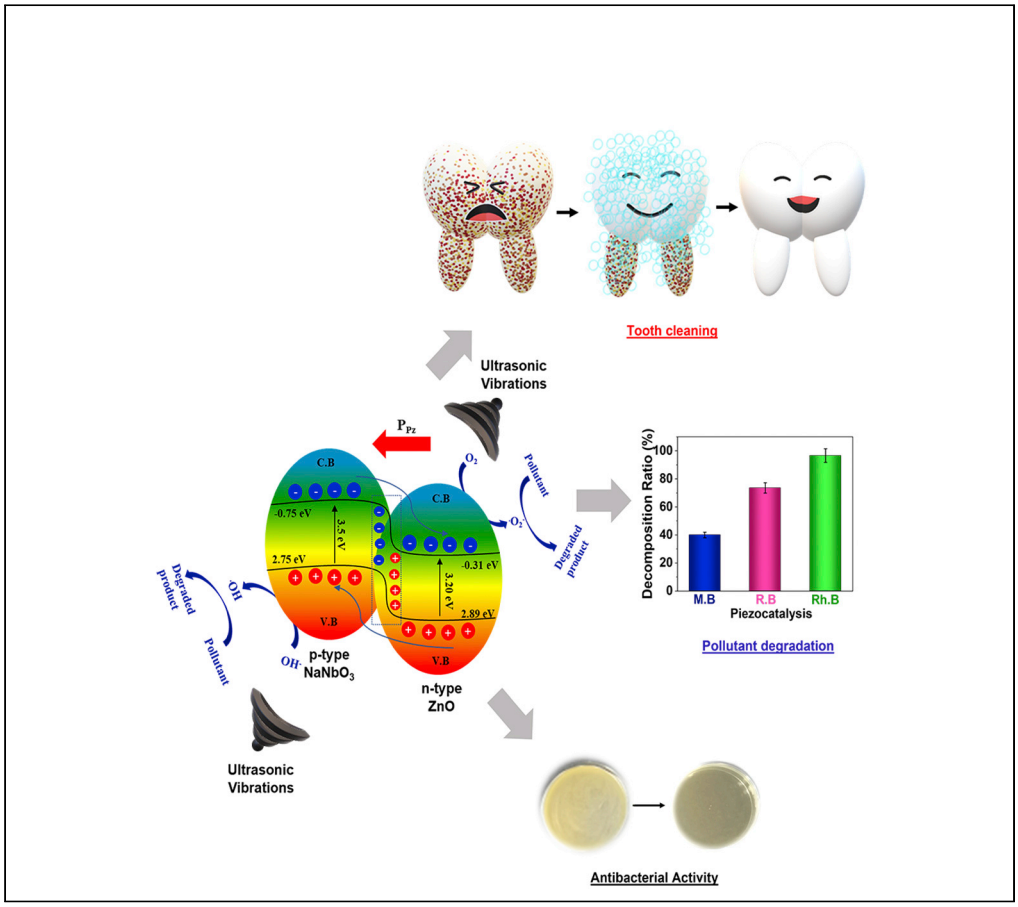

Aditi Sharma, Upasana Bhardwaj, Devendra Jain, Himmat Singh Kushwaha

himmatsingh.mrc@mnit.ac.in

Highlights

$NaNbO_3$/ZnO binary nanocomposite was synthesized by hydrothermal method

$NaNbO_3$/ZnO binary nanocomposite was evaluated as a piezocatalyst

The formation of p-n heterojunction enhances the catalytic activity

$NaNbO_3$/ZnO binary nanocomposite can be used for non-destructive tooth cleaning

Sharma et al., iScience 25, 104915
September 16, 2022
https://doi.org/10.1016/j.isci.2022.104915

iScience

CellPress
OPEN ACCESS

Article

$NaNbO_3$/ZnO piezocatalyst for non-destructive tooth cleaning and antibacterial activity

Aditi Sharma,[1] Upasana Bhardwaj,[1] Devendra Jain,[2] and Himmat Singh Kushwaha[1,3,*]

SUMMARY

Tooth discoloration and plaque formation are serious issues for dental healthcare professionals across the world. Although traditional hydrogen peroxide-based cleaning methods are efficient, they can cause enamel demineralization, periodontal irritation, and toxicity. Also, these treatments are time-taking. Here, we present a noninvasive, safe, and simple tooth cleaning approach by using the piezoelectric phenomenon. After 6 h of vibrations, contaminated teeth can be significantly cleaned by the $NaNbO_3$/ZnO binary nanocomposite. Moreover, the $NaNbO_3$/ZnO binary nanocomposite-based piezocatalysis tooth cleaning procedure causes far less harm to enamel and biological cells in comparison to hydrogen peroxide-based cleaning methods. To evaluate its functionality, organic dyes were degraded by piezoelectric effect of $NaNbO_3$/ZnO binary nanocomposite under ultrasonic irradiation. The piezoelectric potential of $NaNbO_3$/ZnO was found to be 3.75 V. The binary nanocomposite's antibacterial activity was proven to be efficient against *Escherichia coli* with the inhibitory zone of 21 mm and complete removal of bacteria.

INTRODUCTION

Many people are keen to enhance their look with a brighter smile as the aesthetic standard rises. As a result, teeth whitening has become one of the most popular cosmetic dental operations (Alqahtani, 2014). Discoloration and darkening of teeth can be triggered by a variety of factors, including cigarette usage, tobacco, intake of chromogenic foods and beverages (tea and coffee), cold drinks, and ingesting specific flavorings along with poor mouth hygiene (Colares et al., 2019). Staining on teeth is due to the chromogenic substances, which can be produced by the non-enzymatic darkening reaction involving amino acid and sugars or obtained by the preservation of foreign chromophores. In contrast, a polluted tooth provides a fertile and non-shedding environment for bacterial colonization which can lead to or worsen a variety of dental disorders such as enamel demineralization, dental plaque, periodontitis, and dental caries (Dewhirst et al., 2010; Lamont et al., 2018; Lamont and Egland, 2014; Zhang et al., 2019).

There are various typical teeth whitening procedures, professional cleanup and polishing, caps or dentures, regular brushing teeth with aggressive toothpaste, and bleaching, to achieve a cheerful smile (Soeteman et al., 2018). Though, these procedures need the assistance of a competent dentist and may result in irreparable enamel damage (Jung et al., 2012; Kimyai et al., 2017). In comparison to these expensive physical brightening procedures, chemical bleaching technique offers a less expensive option for teeth brightening (Soeteman et al., 2018; Kwon and Wertz, 2015; Carey, 2014). Oxidative bleaching chemicals, particularly hydrogen peroxide, have been frequently used in clinical setups for teeth whitening (Román-Rodríguez et al., 2020). Although this procedure is quite effective, whitening with hydrogen peroxide can have major adverse effects, including as destruction of organic structure and increased dental micro-roughness. Due to this, H_2O_2 favors bacterial recolonization and re-staining (Markovic et al., 2007; Tredwin et al., 2006; Wongpraparatana et al., 2018). Chemical bleaching technique is based on the breakdown of chromogen by the formation of ROS (reactive oxygen species) mainly OH· radicals generated by hydrogen peroxide (H_2O_2), as H_2O_2 produces high amount of OH· which damages the tooth enamel (Kawamoto and Tsujimoto, 2004). This method implies that a substance which can stimulate and emit ROS might be useful as a tooth cleaning agent.

Based on the above principle, Wang et al. presented a tooth whitening technique based on piezocatalysis effect. Under the mechanical vibration, piezoelectric $BaTiO_3$ nanoparticles might create ROS (hydroxide

[1]Materials Research Centre, Malaviya National Institute of Technology Jaipur (MNITJ), India

[2]Department of Molecular Biology and Biotechnology, Maharana Pratap University of Agriculture and Technology, Udaipur, India

[3]Lead contact

*Correspondence: himmatsingh.mrc@mnit.ac.in

https://doi.org/10.1016/j.isci.2022.104915

radical (OH·), superoxide radical ($\cdot O_2^-$)) and destroy organic pigments (Wang et al., 2020b). Zhang et al. proposed that the blue light-activated photocatalysis effect in TiO_2 nanoparticles may be employed for efficient and non-destructive tooth cleaning (Zhang et al., 2018). Zhang et al. also proposed photodynamic non-destructive tooth cleaning technique (Zhang et al., 2021). As compared to the traditional hydrogen peroxide treatment method, this technique is non-destructive, but might cause numerous photo-allergic and photo-toxic reactions, which can result in oral tissue injury. As a result, an efficient, non-destructive, and hygienic tooth cleaning technique that does not require excess time during our regular activities is in high demand.

The piezoelectric effect occurs due to the accumulation of electric charge on the surface of non-centrosymmetric ceramics under the effect of mechanical vibrations. Some examples of piezoelectric materials are $BaTiO_3$ (Wang et al., 2020b), ZnO (Ma et al., 2019), and $NaNbO_3$ (You et al., 2018), which have been reported as an excellent piezocatalyst. ZnO is among the most appealing semiconductor for breaking down organic contaminants because of its ease of manufacture, low cost, non-toxicity, high chemical stability, and great redox ability (Mohd Adnan et al., 2016; Li et al., 2013; Wang et al., 2018). Furthermore, zinc oxide (ZnO) is widely recognized as a safe compound for animals and humans, and it has been widely employed in the manufacture of personal care goods (Perelshtein et al., 2009). Whereas sodium niobate ($NaNbO_3$) also possesses strong chemical stability, low cost, non-toxicity, and good charge carrier mobility. The estimated piezoelectric coefficient (d_{33}) is 12 pmV^{-1} for $NaNbO_3$ (Wang et al., 2012).

Here, we designed a piezocatalytic system that uses two-step hydrothermal technique to produce a p-n heterojunction binary nanocomposite architecture with increased piezocatalytic activity. The experimental findings reveal that the $NaNbO_3$/ZnO binary nanocomposite architecture has outstanding deterioration behavior under ultrasonic vibration action, with greater catalytic efficiency than ZnO and $NaNbO_3$. Based on the above findings, tooth cleaning experiment was conducted, and it was found that the contaminated tooth was cleaned with $NaNbO_3$/ZnO binary nanocomposite in 6 h without any enamel surface damage. Moreover, $NaNbO_3$/ZnO binary nanocomposite possesses an excellent antibacterial activity toward *Escherichia coli* with inhibitory zone of 21 mm.

RESULTS AND DISCUSSION

Structural and morphological characterization of ZnO, $NaNbO_3$, and $NaNbO_3$/ZnO binary nanocomposite

Figure 1A depicts the XRD patterns of ZnO, $NaNbO_3$, and $NaNbO_3$/ZnO binary nanocomposite. In the shown figure, the peaks occurred at 2Θ = 31.70°, 34.31°, 36.27°, 47.57°, 56.48°, 62.79°, 66.27°, 68.01°, 69.09°, 72.57°, and 76.92° were matched well with the hexagonal ZnO crystalline structure (Database no: 36–1451), which belongs to the space group of P63mc and has lattice parameters of a = 3.24 Å, b = 3.24 Å, and c = 5.2 Å (Johar et al., 2015; Mohd Adnan et al., 2016). In the given figure, the characteristic peaks occurred at 2Θ = 22.67°, 32.42°, 38.11°, 40.06°, 46.37°, 52.45°, 57.89°, 67.89°, 72.67°, and 77.24° were mapped well with the Database no: 082–0606, single orthorhombic phase of $NaNbO_3$, with a lattice parameter of a = 7.79 Å, b = 5.51 Å, and c = 5.56 Å (Ji et al., 2014; You et al., 2018). In XRD of $NaNbO_3$/ZnO binary nanocomposite, no further peaks were identified except for ZnO and $NaNbO_3$, indicating that the prepared sample's compositions were $NaNbO_3$ and ZnO.

Structural quality, structural flaws, and disorders may affect the Raman spectra of fabricated materials. Figure 1B shows the Raman spectra of ZnO, $NaNbO_3$, and $NaNbO_3$/ZnO binary nanocomposite. The spectra were recorded at room temperature using a 532 nm laser source. In the Raman spectra of ZnO, the high-intensity peak arises at 438 cm^{-1}, which correlates with the E_2(high) vibrational modes of oxygen. The second order phase is linked with the peak arises at 330 cm^{-1}, which correlated with the discrepancy between E_2(high) and E_2(low). A_1(TO) modes are responsible for the peak arises at 330 cm^{-1} (Ngo-Duc et al., 2012). The development of defects such as oxygen vacancies (V_O) or other faulty forms was linked to the conspicuous peak at 661 cm^{-1} assigned to the E_1(LO) mode of ZnO (Šćepanović et al., 2010). In $NaNbO_3$ Raman spectra, the intrinsic modes of NbO_6 in $NaNbO_3$ are featured in the peaks from 150 cm^{-1} to 1000 cm^{-1}. The region spanning 150 cm^{-1} to 300 cm^{-1} is associated with the triply degenerated v_5 (F_{2g}) and v_6 (F_{2u}) (Ji et al., 2014). The NbO_6 spinning caused the peak to emerge at 139 cm^{-1}. The peak at 433 cm^{-1} correlates with v_5 (F_{1u}). The peak which is appeared at 602 cm^{-1} corresponds to v_1 ($A1_g$) (Shen et al., 1998). Furthermore, the peak appeared at 870 cm^{-1} verifies the ABO_3 structure formation (Huan et al., 2015). The Raman spectra of $NaNbO_3$/ZnO binary nanocomposite exhibit both ZnO as well as $NaNbO_3$.

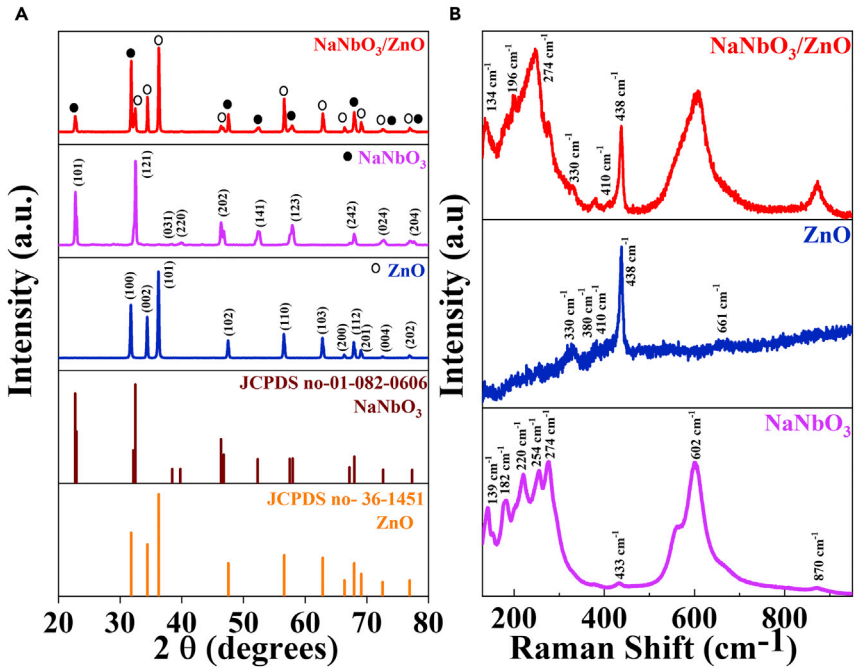

Figure 1. Structural characterization of prepared materials

(A) XRD patterns for ZnO, $NaNbO_3$, and $NaNbO_3$/ZnO binary nanocomposite and (B) Raman spectra of ZnO, $NaNbO_3$, and $NaNbO_3$/ZnO binary nanocomposite.

To evaluate the composition and component elemental valence state of the synthesized materials, X-ray photoelectron spectroscopy (XPS) was performed for $NaNbO_3$/ZnO sample. Figure 2A shows the survey spectra which clearly display the characteristic peaks of Zn 2p, Nb 3d, Na 1s, and O 1s, indicating the existence of these components in the binary nanocomposite. Figures 2B–2E display the high-resolution spectrum for the elements in $NaNbO_3$/ZnO. In the Zn 2p range, the bond energies for Zn $2p_{3/2}$ and Zn $2p_{1/2}$ arise at 1022.26 and 1045.38 eV, respectively, which are compatible with the valence of Zn^{2+}(Sharma et al., 2022). At the very same moment, the binding energies of 206.55 and 209.32 eV are attributed to Nb $3d_{5/2}$ and Nb $3d_{1/2}$, which corresponds to the Nb^{5+} oxidation state (Saha et al., 2018). The typical bond energy of 1071.15 eV exhibited by Na 1s, which corresponds to the Na^{1+} oxidation state, which is well comparable with published data (Xu et al., 2011). The binding energy associated with 1070.8 $\pm$ 0.05 was related to Na ions that formed in the perovskite lattice (Molak et al., 2009). While, the O 1s orbital peak splits into two peaks which is observed at 531.07 and 532.25 eV, which is caused by the structural oxygen embodied by the sodium niobate and zinc oxide as well as the adsorbed oxygen generated by the sample when exposed to the environment (Claros et al., 2020).

To examine the morphology of the binary nanocomposite, scanning electron microscopy (SEM) was utilized to examine ZnO, $NaNbO_3$, and $NaNbO_3$/ZnO materials. As shown in Figure 3A, from an entire microscopic view, ZnO is composed of rod-like morphology with length in several micrometers and a diameter of 30–100 nm, and the surface of ZnO nanorods is smooth (Ma et al., 2019). Figure 3B is the SEM micrograph of the synthesized $NaNbO_3$. The picture reveals that the $NaNbO_3$ is composed of rod-like morphology with the diameter in micrometer range with clean surface (Kumar and Khare, 2017). Figure 3C is the SEM micrograph of $NaNbO_3$/ZnO binary nanocomposite. From the given figure, it is clear that the ZnO nanorods are homogeneously dispersed on the $NaNbO_3$ nanorods of larger size. In addition, the findings of the EDS elemental mapping are shown in Figures 3D–3H, which clearly indicate the presence of Zn, Nb, Na, and O, providing preliminary evidence for the effective production of binary nanocomposite piezocatalytic materials, which was in accordance with the XRD findings.

Optical properties

Ultraviolet-visible diffuse reflectance spectroscopy (UV–vis DRS) of $NaNbO_3$, ZnO, and $NaNbO_3$/ZnO is depicted in Figure 4A. Simultaneously, the DRS spectra are utilized to compute the connection between

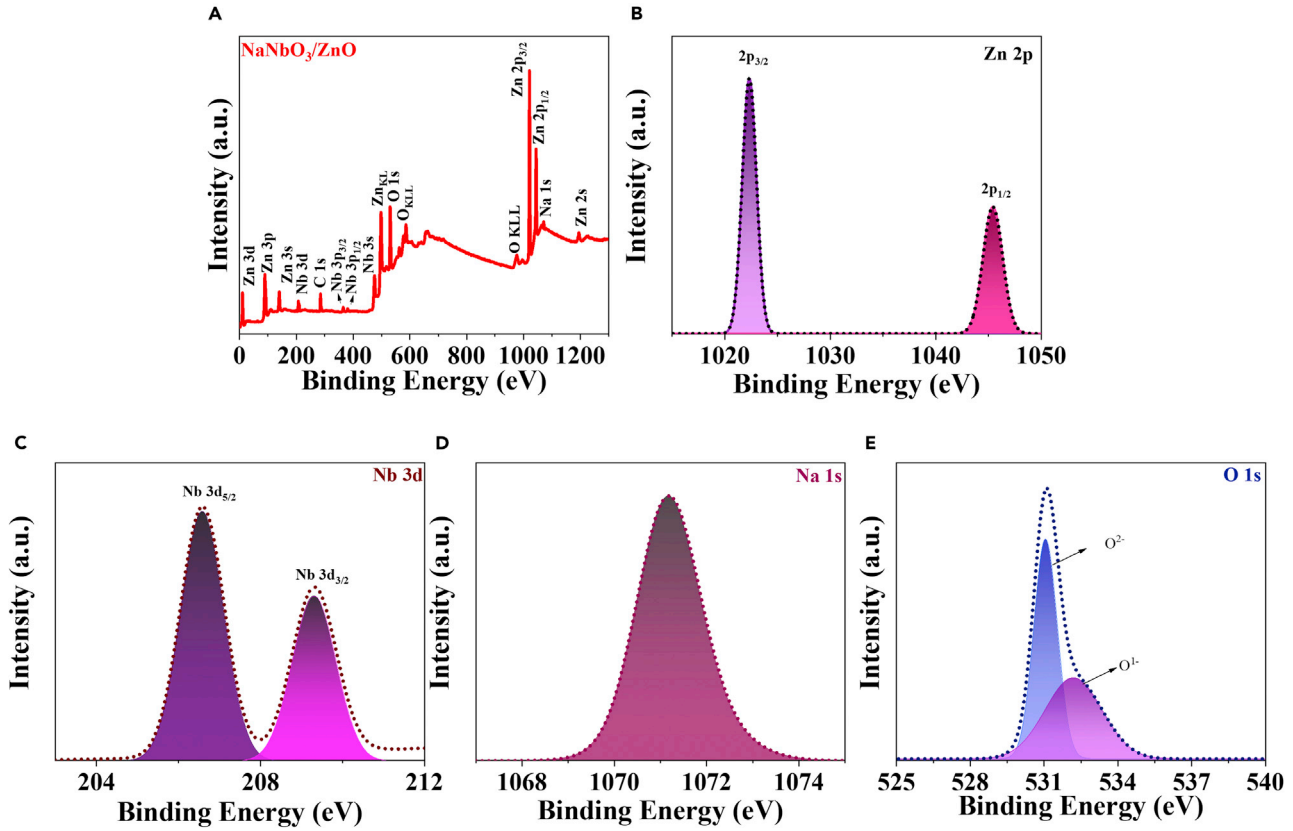

Figure 2. XPS analysis of $NaNbO_3$/ZnO

XPS analysis of $NaNbO_3$/ZnO, (A) XPS survey, (B) High-resolution spectra of Zn 2p, (C) High-resolution spectra of Nb 3days, (D) High-resolution spectra of Na 1s, and (E) High-resolution spectra of O 1s.

photon energy (hυ) and $(\alpha h\upsilon)^2$ to evaluate the bandgap (E_g) of the synthesized materials as shown in Figures 4B–4D. The E_g values of ZnO, $NaNbO_3$, and $NaNbO_3$/ZnO are determined to be 3.20 (Li et al., 2019), 3.6 (Wang et al., 2012), and 3.15 eV, respectively, by using tauc plot. The decrease in bandgap was observed due to the formation of interfaces.

Piezoresponse force microscopy analysis

Piezoresponse force microscopy measurement was employed to validate the piezoelectric polarization in $NaNbO_3$/ZnO binary nanocomposite as a function of bias voltage. Initially, $NaNbO_3$/ZnO binary nanocomposite was coated over the ITO substrate, and then measurement was performed in a contact mode. When $\pm$10 voltage is applied to the material, the phase plot represents the formation of polarization in the material. Whereas amplitude plot depicts the formation of strain in the material (Pan et al., 2013). Figure S2A indicates that there is not any significant change in the phase when there is no bias voltage; however, polarization occurs when voltage is applied, as indicated in Figure S2B. Figures S1C and S1D show the amplitude image. The appropriate phase and amplitude patterns are shown in Figure S2D. Figure S1E displayed the appropriate phase and amplitude patterns. As the saturation voltage approached to 10 V, a butterfly loop showed a maximum value of 0.95 mV, showing that the $NaNbO_3$/ZnO binary nanocomposite possesses exceptional piezoelectric properties (Ji et al., 2014). The phase hysteresis is directly linked to the orientation of the electric dipole moments. As a result, the swapping of dipoles is pushed to align with the direction of applied electric field. This phase swapping clearly shows ferroelectricity (Kumar et al., 2021).

Piezocatalytic performance of ZnO, $NaNbO_3$, and $NaNbO_3$/ZnO binary nanocomposite

To show the higher piezoelectric effect on the catalytic activity of $NaNbO_3$/ZnO binary nanocomposite, the prepared samples (ZnO, $NaNbO_3$, and $NaNbO_3$/ZnO) were independently examined by the

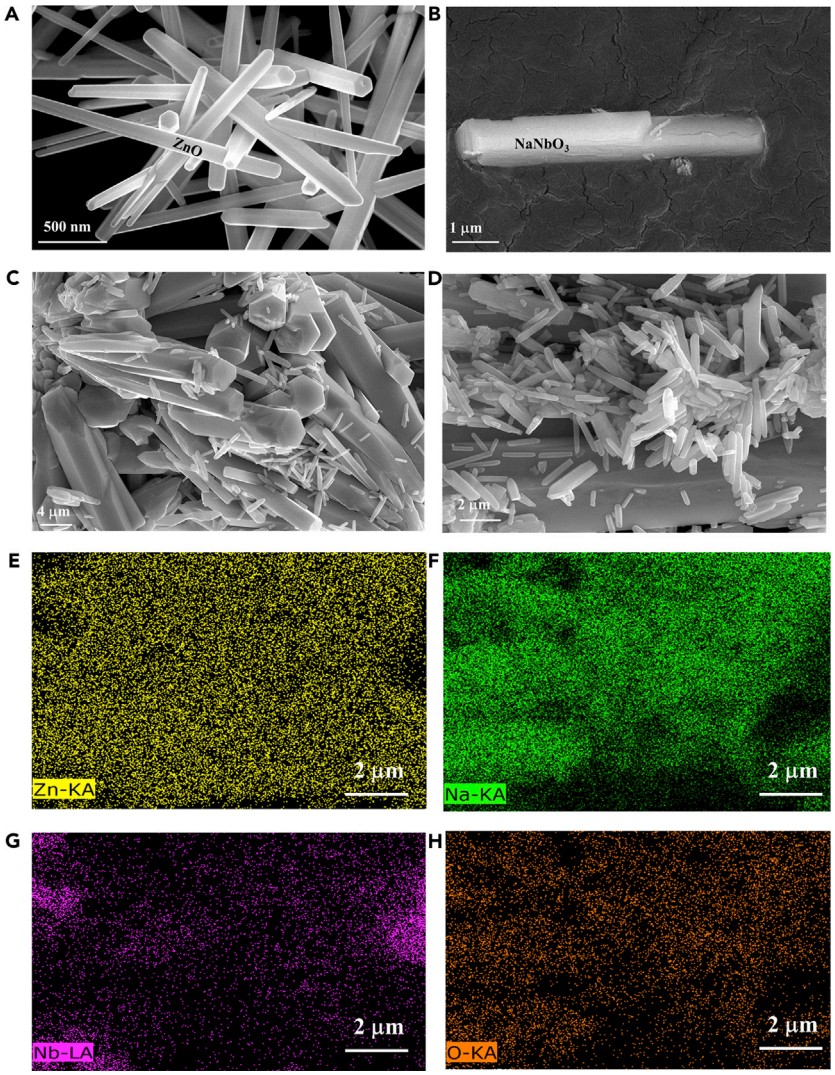

Figure 3. Structural and elemental characterization

(A) ZnO, (B) $NaNbO_3$, and (C) $NaNbO_3$/ZnO binary nanocomposite, (D–H) elemental mapping photographs of $NaNbO_3$/ZnO binary nanocomposite.

decomposition efficiency for rhodamine b with ultrasonic circumstances (Sharma et al., 2021b). As illustrated in Figures 5A and 5B, the degrading efficiency of ZnO, $NaNbO_3$ to rhodamine b in 5 min is less than 25% under reaction circumstances of 60 min of ultrasonic vibrations, but the $NaNbO_3$/ZnO binary nanocomposite (Figure 5C) exhibits a significantly greater efficiency of 88.57% in just 5 min. The degrading performance of the hybrid material demonstrates that the coupling of the piezoelectric materials $NaNbO_3$ and ZnO materials can accelerate the degradation of rhodamine b. Figure 5D shows the overall decomposition ratios of rhodamine b treated with different catalyst under the ultrasonic conditions. Within 60 min of reaction time, ZnO degraded only 48.49% of rhodamine b organic dye and $NaNbO_3$ degraded 84.95% of rhodamine b organic dye, whereas the combination of these two materials degrades rhodamine b organic dye up to 97%. The standardize concentration graph is shown in Figure 5E, which are generated by the difference in the absorbance peak at distinct time periods (Singh and Khare, 2017). The associated rate constant was calculated by fitting the empirical findings according to the pseudo first-order kinetic rate equation ($\ln kt = C/C_0$) as depicted in Figure 5F. The standardize concentration and rate constant graphs clearly show an increase in the decomposition rate when subjected to ultrasonic vibrations with $NaNbO_3$/ZnO binary nanocomposite. It was found that there is substantial increase in the piezocatalytic degradation rate utilizing $NaNbO_3$/ZnO binary nanocomposite compared to ZnO and $NaNbO_3$ solely (Xue et al., 2015).

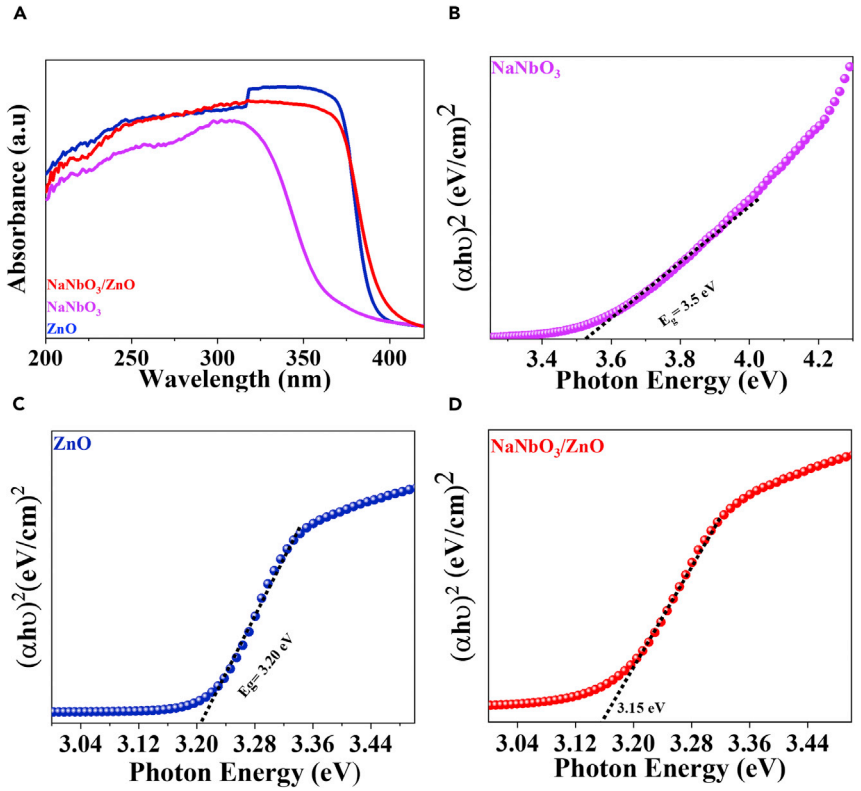

Figure 4. Optical charracterization and bandgap analysis

(A) UV-vis absorption spectra for ZnO, $NaNbO_3$, and $NaNbO_3$/ZnO, (B–D) Tauc plots for $NaNbO_3$, ZnO, and $NaNbO_3$/ZnO samples.

Furthermore, the value of the rate constant (k) follows the layout of the deterioration performance curve. The result demonstrates that the binary nanocomposite material has a strong catalytic effect under mechanical vibrations, with the tremendous breakdown efficiency and the highest rate constant. The deterioration impact of the $NaNbO_3$/ZnO binary nanocomposite ($k = 5.1x10^{-2}$ min^{-1}) under ultrasonic conditions is higher than that of ZnO ($k = 6x10^{-3}$ min^{-1}) and $NaNbO_3$ ($k = 3.12x10^{-2}$ min^{-1}). The reaction rate of $NaNbO_3$/ZnO binary nanocomposite is enhanced by 8.5 times than ZnO and 1.7 times than $NaNbO_3$. The rate order cure of different catalyst is shown in Figure S3.

Furthermore, to examine the degradation efficiency of binary nanocomposite, different targeted pollutants were used for the degradation under piezoelectric effect. Figures 6A–6C are the UV absorbance spectra for methylene blue (cationic dye), rose bengal (anionic dye), and rhodamine b (cationic dye). For methylene blue dye, the UV-vis absorbance spectra have a peak at 663 nm. When the duration of mechanical vibration prolonged, the absorption strength of methylene blue dropped, confirming that the degradation of the methylene blue dye employed with binary nanocomposite (Figure 6A). Within 60 min of exposure time, methylene blue degrades slowly. For rose bengal, the UV-vis absorbance spectra have a peak at 265 nm. Within 60 min of exposure time, rose bengal degrades moderately. When the duration of mechanical vibration prolonged, the absorption strength of rose bengal dropped, confirming that the degradation of the rose bengal dye employed with $NaNbO_3$/ZnO binary nanocomposite (Figure 6B). Figure 6C shows the UV-vis spectra for rhodamine b, the graph indicates that, when the duration of mechanical vibration increased, the absorption strength of rhodamine b decreased, confirming that the degradation of the rhodamine b dye employed with binary nanocomposite. Within 60 min of exposure time, rhodamine b degrades rapidly. Figure 6D shows the overall decomposition ratios of different pollutant treated with binary nanocomposite under the ultrasonic conditions. Within 60 min of reaction time, methylene blue degrades only up to 40%, rose bengal degrades only up to 73.75%, and rhodamine b degrades up to 97%. Figure 6E is the degradation efficiency curve, which was calculated by the difference between the initial concentration and concentration obtained by the treatment. Figure 6F depicts the associated rate constant was

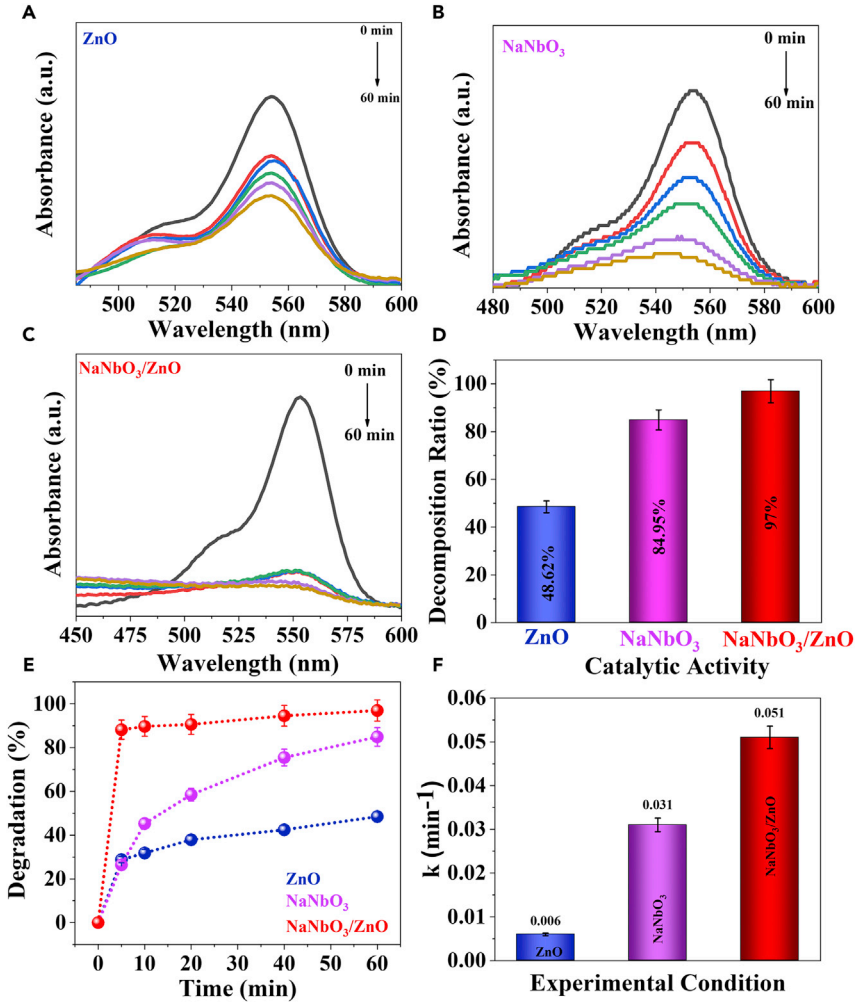

Figure 5. Piezocatalytic degradation performance of prepared samples for the degradation of rhodamine b organic dye

(A) ZnO, (B) $NaNbO_3$, (C) $NaNbO_3$/ZnO binary nanocomposite, (D) decomposition ratio for the different piezocatalyst, (E) Piezocatalytic degradation efficiency curve, (F) Comparative evaluation of the rate constant. Each curve and bar is the mean and standard deviation of at least three replicates.

calculated by fitting the empirical findings according to the pseudo first-order kinetic rate equation (ln kt = C/C_0). Furthermore, the rate constant (k) value follows the layout of the deterioration performance curve. The result demonstrates that the binary nanocomposite material has a strong catalytic effect under mechanical vibrations, with the tremendous breakdown efficiency and the highest rate constant. The deterioration impact of the rhodamine b ($k = 5.1 \times 10^{-2}$ min^{-1}) under ultrasonic conditions is higher than that of rose bengal ($k = 2 \times 10^{-2}$ min^{-1}) and methylene blue ($k = 4.7 \times 10^{-3}$ min^{-1}). From the observations, it is concluded that this binary nanocomposite can be used for both cationic and anionic dyes.

Electrochemical measurements

The ZnO, $NaNbO_3$, and $NaNbO_3$/ZnO were utilized as piezo anodes for rapid piezo current response studies to examine the cause for the reported increase in catalytic performance of the $NaNbO_3$/ZnO binary nanocomposite. As reveled in Figure 7A, the photocurrent density of $NaNbO_3$/ZnO binary nanocomposite is considerably greater than solitary ZnO and solitary $NaNbO_3$, which indicate that the binary nanocomposite material has increased charge carrier separation performance and high electron mobility. It can be utilized as an effective piezoelectric active catalyst. In addition, the electrochemical impedance spectroscopy

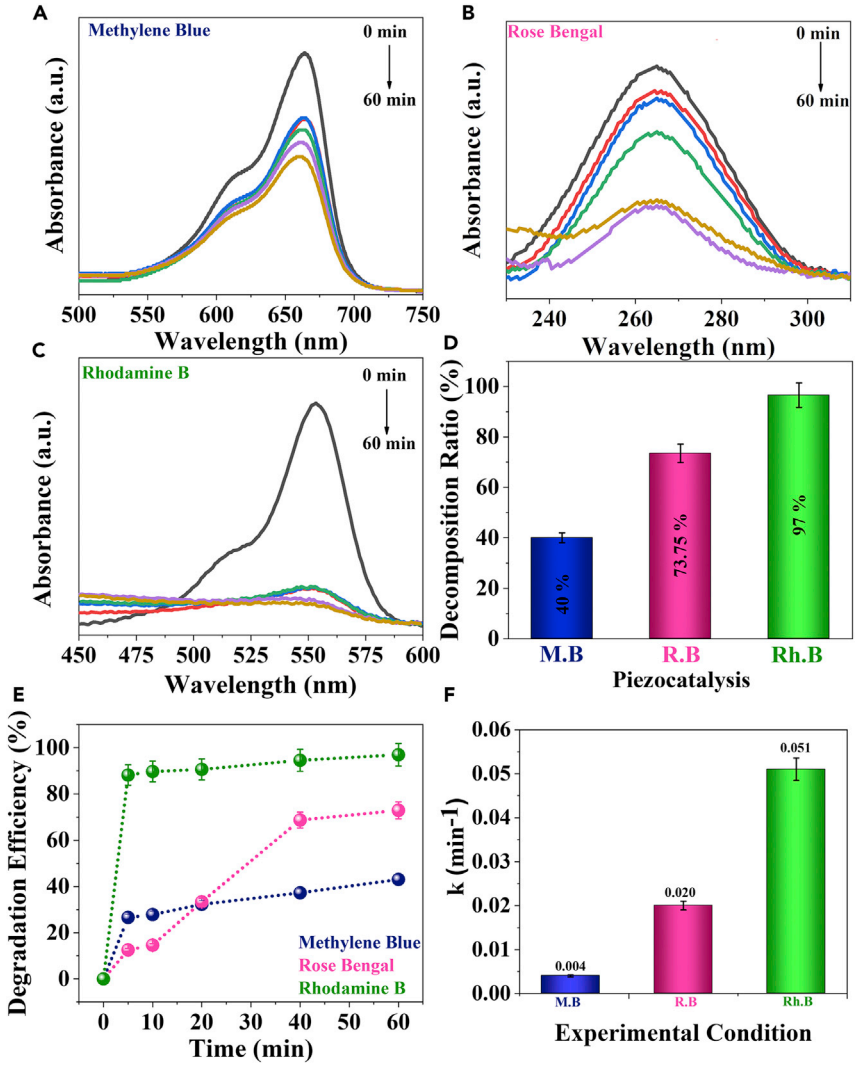

Figure 6. Piezocatalytic degradation performance of $NaNbO_3$/ZnO binary nanocomposite for the degradation

(A) Methylene Blue, (B) Rose bengal, (C) rhodamine b organic dye, (D) decomposition ratio for the different pollutant, (E) Piezocatalytic degradation efficiency curve, (F) Comparative evaluation of the rate constant for the different pollutants. Each curve and bar is the mean and standard deviation of at least three replicates.

was used to examine the charge transport mechanism of ZnO, $NaNbO_3$, and a $NaNbO_3$/ZnO binary nanocomposite. The binary nanocomposite has lower arc radius than ZnO and $NaNbO_3$, as shown in Figure 7B. It demonstrates that the electrical resistance of the charge transport mechanism in two-layer composite is smaller, i.e. 371.9 Ω than that of ZnO (470.9 Ω) and $NaNbO_3$ (420.4 Ω) (Sharma et al., 2021c). The smaller charge transfer resistance in binary nanocomposite results into high electron mobility which promotes high catalytic activity by increasing the charge carriers. Figure 7C shows generated piezo potential of $NaNbO_3$/ZnO binary nanocomposite measured by digital scanning oscilloscope (DSO). When the pallet of $NaNbO_3$/ZnO binary nanocomposite was placed under the ultrasonic vibrations, the potential was created in response to the vibrations and gives positive voltage. In contrast, when the stress was released from the pallet by turning off the ultrasonic vibrations, it shows negative voltage which indicates that the stress was removed from the binary nanocomposite. And the piezo potential recorded was 3.75 V as shown in Figure 7C. Whereas similar trend was observed when the stress was applied by manual tapping, and the recorded voltage is shown in Figure 7D, which is 1.86 V. Even though our thumb inserted the stress here, the unmanaged conditions of applied and withdrew pressure may only result in certain irregularities of negative and positive signals.

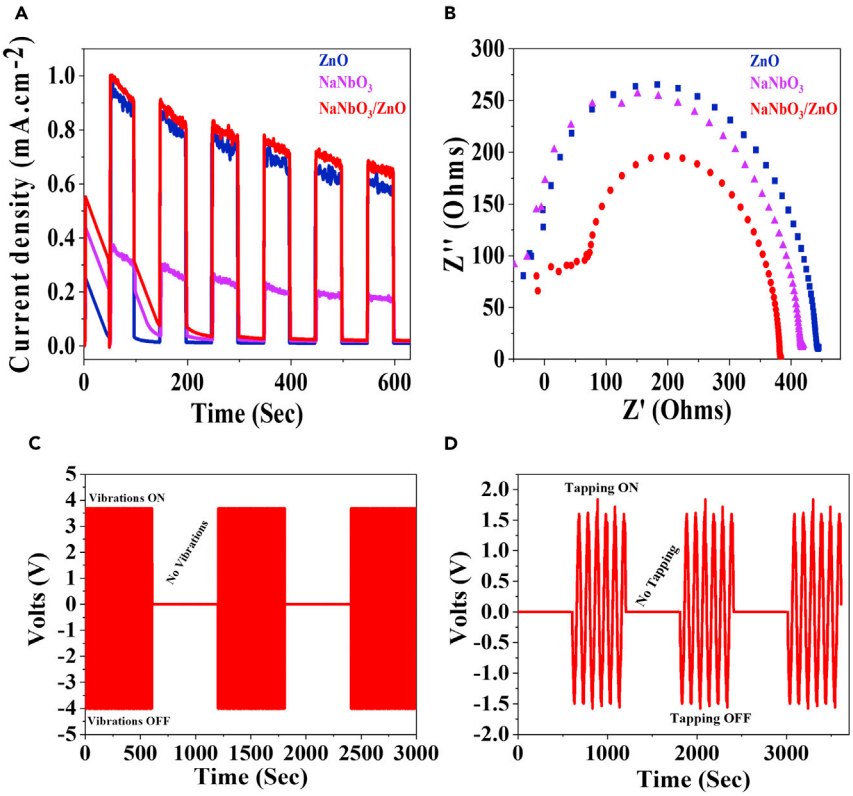

Figure 7. Piezocurrent and Piezopotential analysis

(A) Transient piezo current response, (B) EIS analysis for different prepared samples, Piezo-potential formation (C) under ultrasonic vibrations, and (D) with hand tapping.

Scavenging test

With scavenger studied, the piezocatalytic reaction pathway for binary nanocomposite was investigated in this work. To discover the major active components in the piezocatalytic mechanism, the utilized capturing agents are: Isopropanol alcohol (IPA: for OH· radical), 2Na-ethylenediamine tertraacetic acid (2Na-EDTA: for h^+), and *para*-Benzoquinone (BQ: for $\cdot O_2^-$) (Wang et al., 2020a). As displayed in Figure 8A, when 2Na-EDTA, IPA, and BQ were added to the reaction mixture, the piezoelectric catalytic degradation efficiency of the rhodamine b solution decreased from 97% to 18.01%, 53.38%, and 11.91%, respectively, demonstrating that holes, hydroxyl radicals, and superoxide radicals are the primary active material responsible for the piezoelectric catalytic process. Moreover, to further explore the catalytic mechanism, photoluminescence (PL) spectroscopy was used to identify the generated OH radicals. For hydroxyl radical detector, terephthalic acid was utilized as a probe. Terephthalic acid rapidly combines with OH· radical to produce the extremely luminous compound 2-hydroxyterephthalic acid. The method concentrates on the PL signals generated at the water-$NaNbO_3$/ZnO contact at 425 nm. The formation of 2-hydroxyterephthalic acid is directly proportional to the concentration of OH· radical generated during piezocatalysis. Figure 8B displayed the PL spectrum of terephthalic acid with binary nanocomposite solution under mechanical vibrations with increasing irradiation duration.

Piezocatalysis mechanism

The piezocatalytic process for $NaNbO_3$/ZnO binary nanocomposite has been deduced relying on the foregoing investigation, and the related mechanism is presented in Figure 9. In the n-type ZnO, the free electron (e^-) population is greater than the hole (h^+) population, but in p-type $NaNbO_3$ the hole (h^+) population is greater than the free electron (e^-) population (Lee et al., 2018; Liu et al., 2019). Figure 9 shows how the p-type $NaNbO_3$ and n-type ZnO create a heterojunction architecture at the contact region, establishing inner electric fields on both faces to improve the separation of electron and hole couples. The carriers in the $NaNbO_3$/ZnO binary nanocomposites will recombine if the piezoelectric polarization was not present.

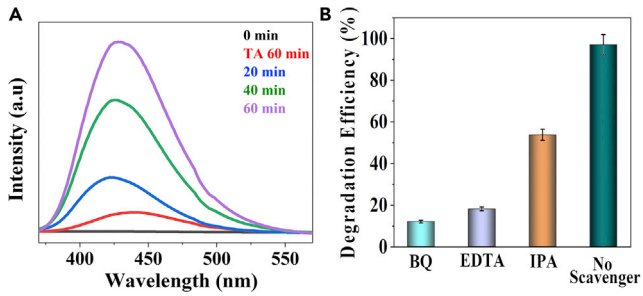

Figure 8. Scavenging analysis

(A) Photoluminescence spectra for hydroxyl radical (●OH) detection and (B) Trapping study for active species employing piezocatalysis.

In response to ultrasonic vibrations, the holes and electrons inside the crystals will face spontaneous polarization in $NaNbO_3$ and ZnO material. The band alignment of the p-n junction tilted more than those solely triggered by heat-excited free charges. During mechanical vibrations, the electrons (e^-) present in the valence band of the ZnO were stimulated to the conduction band leaving behind holes in valence band, due to arrangement of the band energy. The holes present in the valence band of ZnO could migrate to the $NaNbO_3$ valence band through the depletion region between ZnO and $NaNbO_3$ because polarized negative charges will attract holes in ZnO. In contrast, the polarized positive charges will attract electrons in $NaNbO_3$. Throughout the migration phase, the adsorbed oxygen interacts with electron to convert it into super oxide radical ($\cdot O_2^-$). Simultaneously, this superoxide radical will interact further with -OH to create OH· radical, which will contribute to the oxidation process. Whereas holes in the valence band interact with water to produce OH· radical, this will further involve in oxidation process (Chen et al., 2019). The developed material architecture accelerates carrier mobility, prevents the recombination of holes and free electrons, and inhibits the aggregation of holes and electrons, resulting in much more electrons and holes to engage in the degrading process. According to the results of the foregoing study, the $NaNbO_3$/ZnO binary nanocomposite architecture for cooperative catalysis can successfully carry out carrier segregation and mobility, resulting in redox reactions (1–4).

$$NaNbO_3/ZnO + \text{Ultrasonic Vibrations } NaNbO_3\ (h^+) + ZnO\ (e^-) \quad \text{(Equation 1)}$$

$$e^- + O_2 \cdot O_2^- \quad \text{(Equation 2)}$$

$$h^+ + H_2O\ OH\cdot \quad \text{(Equation 3)}$$

$$\text{Pollutant} + (\cdot O_2^-/OH\cdot)\ \text{Dye degradation} \quad \text{(Equation 4)}$$

Tooth cleaning mechanism

Following the confirmation of piezocatalysis activity of $NaNbO_3$/ZnO binary nanocomposite via rhodamine b and rose bengal degradation, a tooth brightening experiment was conducted by employing $NaNbO_3$/ZnO binary nanocomposite. The major causes of tooth discoloration include a high intake in pigmented foods such as tea, coffee, pan masala, cold drink, and juice, as well as poor oral hygiene (Colares et al., 2019). Human-extracted teeth were immersed in a combination of tea, coffee, pan masala, and cold drink for a week to imitate tooth discoloration. Later, the pigmented teeth were processed with a piezoelectric catalytic whitening method in $NaNbO_3$/ZnO binary nanocomposite aqueous solution. As depicted in Figure 10A, the pigmented tooth was all noticeably lightened after being exposed to ultrasonic vibrations for 6 h. Tooth submerged treated with distilled water under ultrasonic vibrations was not lightened due to the absence of piezoelectric $NaNbO_3$/ZnO binary nanocomposite, as shown in Figure 10B. Tooth cleaning experiments were performed using ZnO and $NaNbO_3$ solely, as shown in Figure S4. It was observed that the tooth enamel was cleaned perfectly with ZnO and $NaNbO_3$ within 6 h, but the roots of the tooth were not cleaned properly because roots contain the high concentration of staining agents, and the ROS generated by ZnO and $NaNbO_3$ was comparatively low. Tooth cleaning experiment was also

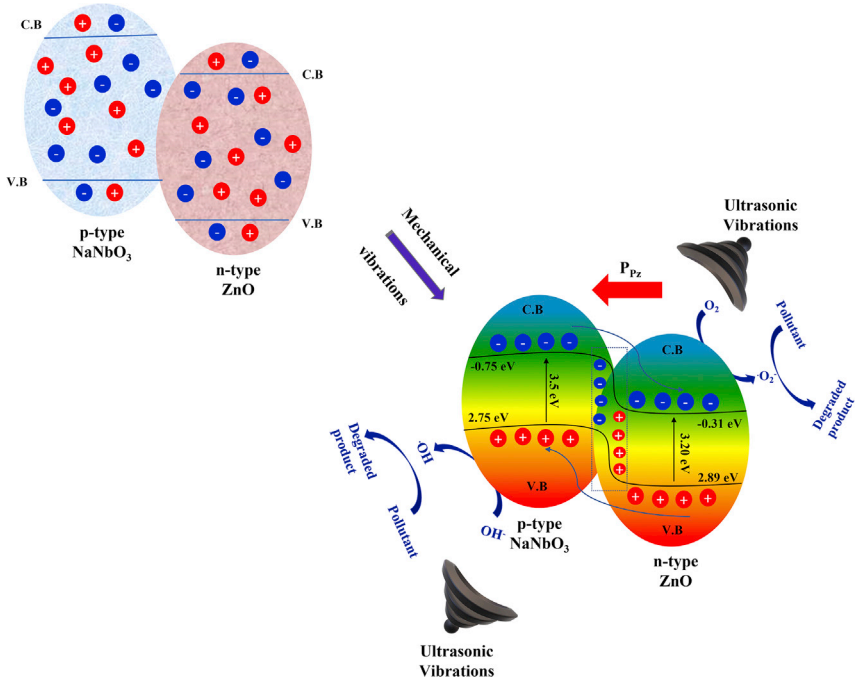

Figure 9. Mechanism for the piezocatalysis process of $NaNbO_3$/ZnO binary nanocomposite

performed by using electric toothbrush as shown in Figure S5. It has been observed that the tooth cleaning by electric toothbrush takes more time than ultrasound system because of two reasons. First, the teeth were not dipped in the binary nanocomposite solution due to which it lacks in the concentration of $NaNbO_3$/ZnO binary nanocomposite around the teeth. Secondly, electric toothbrush has low vibration energy as compared to ultrasound system. This results in the low generation of reactive oxygen species (OH·, $\cdot O_2^-$) on the tooth surface. The morphology of a tooth was photographed before the tooth cleaning experiment to generate a baseline, as depicted in Figure 11A. After the piezocatalysis treatment, the enamel's integrity was assessed using a scanning electron microscope (SEM). It was found that the piezocatalytic tooth cleaning is not damaging the tooth enamel's surface, shown in Figure 11B. In contrast, tooth cleaning with 30% H_2O_2 solution in a standard clinical method for 6 h results in damage to the tooth enamel's surface as impressions and corrosion holes as shown in Figure 11C. In summary, the tooth was lightened as a consequence of a number of chemical processes that result in the destruction of chromogen, a component of chemical interactions involving sugars and amino acids (Alqahtani, 2014). The reactive agents (hydroxyl radical (·OH) and super oxide ion ($\cdot O_2^-$)) formed by $NaNbO_3$/ZnO binary nanocomposite oxidize the numerous conjugated double bonds of big organic substances that cause stains (i.e., chromogen), resulting in smaller complexes (i.e, tooth whitening) (Carey, 2014). These findings imply that the piezocatalysis tooth cleaning via $NaNbO_3$/ZnO binary nanocomposite is noninvasive to tooth surface (Zhang et al., 2021).

Antibacterial activity

Antibacterial activities of the $NaNbO_3$/ZnO binary nanocomposite against *E. coli* were studied by the well diffusion method using a Luria Bertani agar and the 100 μL of 1g L^{-1} $NaNbO_3$/ZnO binary nanocomposite exhibited superior antibacterial activity by producing 21 mm inhibition zone as recorded in Figure 12. The antibacterial activities of $NaNbO_3$/ZnO binary nanocomposite may be attributed to presence of ZnO. It has excellent broad-spectrum antibacterial properties and become the research focus of new antibacterial agents in recent times (Jiang et al., 2020). Furthermore, the antibacterial activities of $NaNbO_3$/ZnO binary nanocomposite were also evaluated as a function of time at which the $NaNbO_3$/ZnO binary nanocomposite was in contact with *E. coli* to kill them completely at different time interval under the piezocatalytic effect (as recorded in Figure 13). The results depicted that the antibacterial activities of $NaNbO_3$/ZnO binary nanocomposites increase with the increasing vibration time. It has been observed that the number of colonies produced on the LB agar medium reduced with increased vibration time. After 60 min of incubation period with consistent shaking at 200 rpm, the $NaNbO_3$/ZnO binary nanocomposite completely eliminated the

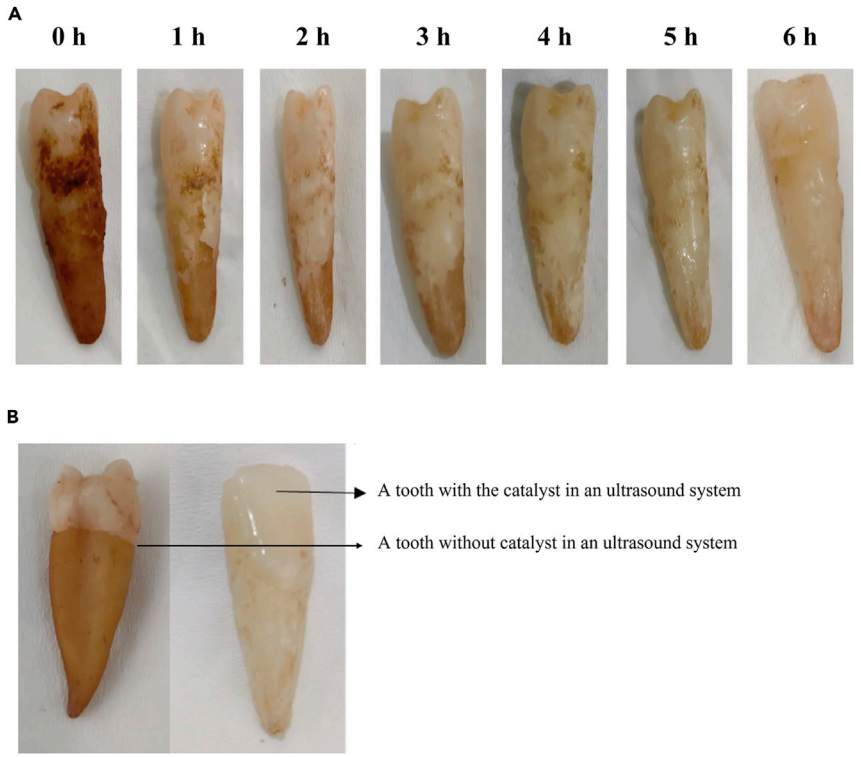

Figure 10. Pictures of the tooth after vibration therapy

(A) Aqueous solution containing $NaNbO_3$/ZnO binary nanocomposite for 0–6 h and (B) Tooth cleaned with or without $NaNbO_3$/ZnO binary nanocomposite.

E. coli. The antimicrobial activities of $NaNbO_3$/ZnO binary nanocomposite may be due to the direct contact of NaNbO3/ZnO binary nanocomposite on the surface of *E. coli*. Previously, Wong et al. reported a similar result with ZnO-based nano-catalyst also supports the finding of the present study. In the present study, $NaNbO_3$/ZnO binary nanocomposite was found to have superior *E. coli* antibacterial activities which could be mostly due to generation of high reactive oxygen species (ROS) resulted in protein denaturation, loss of cell proliferation, and inhibition of cellular respiratory system or microbial cell membrane dysfunction (Jiang et al., 2020).

Antibacterial activities of NaNbO3/ZnO binary nanocomposite against *E. coli* at different incubation time under constant shaking conditions at 37°C temperature was depicted in Table 1.

Conclusion

In summary, $NaNbO_3$/ZnO binary nanocomposite was synthesized by hydrothermal method. The formation of p-n heterojunction promotes the generation of reactive oxygen species (ROS) in large amount under piezoelectric effect. This binary nanocomposite could degrade rhodamine b up to 97% in 60 min of ultrasonic vibrations. The degradation rate constant of $NaNbO_3$/ZnO binary nanocomposite is 5.1 $X10^{-2}$ min^{-1}

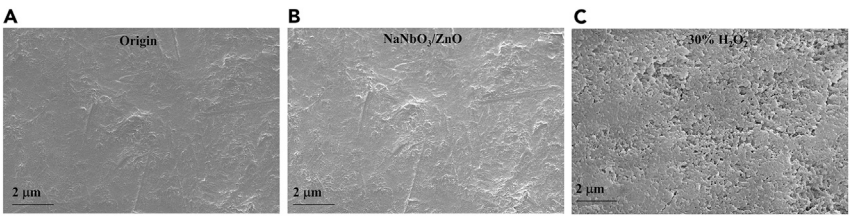

Figure 11. The SEM photographs of a tooth

(A) before experiment, (B) After treatment with $NaNbO_3$/ZnO binary nanocomposite and (C) treatment with 30% H_2O_2.

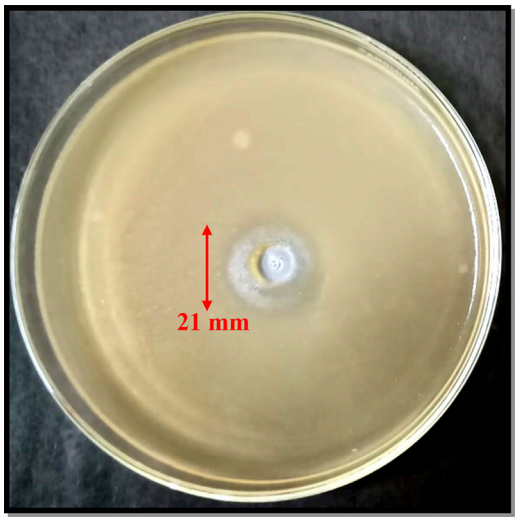

Figure 12. Antibacterial activities of $NaNbO_3$/ZnO binary nanocomposite against *E. coli.* by well diffusion method with $NaNbO_3$/ZnO binary nanocomposite concentration of 1g L^{-1}

which is 8.5 times higher than ZnO and 1.7 time than $NaNbO_3$ solely. This binary nanocomposite can whiten tooth noninvasively contaminated with different beverages. The piezoelectric potential of binary nanocomposite was found to be 3.75 V. The binary nanocomposite's antibacterial activity was proven to be efficient against *E. coli* with inhibitory zone of 21 mm.

Limitation of the study

Tooth cleaning experiments were done in this study by using ultrasonic vibrations which takes hours to clean. To minimize the tooth cleaning time, more studies are needed. Potential avenues of research could include low-frequency piezocatalytic materials with another 2-dimensional morphology, high piezo-potential, and increased polarization.

STAR★METHODS

Detailed methods are provided in the online version of this paper and include the following:

- KEY RESOURCES TABLE
- RESOURCE AVAILABILITY
  - Lead contact
  - Materials availability
  - Data and code availability
- METHOD DETAILS
  - Synthesis of $NaNbO_3$-ZnO binary nanocomposite
  - Piezocatalytic activity experiments
  - Electrochemical measurements
  - Scavenger experiment
  - Piezo-potential measurement
  - Tooth cleaning experiment

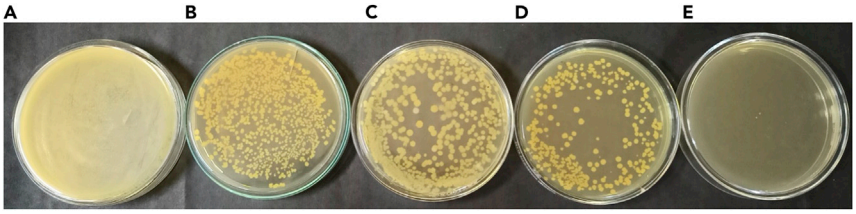

Figure 13. Antibacterial activities of $NaNbO_3$/ZnO binary nanocomposite against *E. coli* at different incubation time under constant shaking conditions

(A) 0 min (B) 15 min (C) 30 min (D) 45 min (E) 60 min.

Table 1. Antibacterial activities of $NaNbO_3$/ZnO binary nanocomposite against *E. coli* at different incubation time under constant shaking conditions at 37°C temperature

Vortex Exposure time (min)	*E. coli* (cfu mL^{-1})
0 min	2.4×10^5
15 min	1.8×10^4
30 min	1.2×10^3
45 min	1.8×10^2
60 min	0

- Antibacterial activity tests
- Materials characterizations

SUPPLEMENTAL INFORMATION

Supplemental information can be found online at https://doi.org/10.1016/j.isci.2022.104915.

ACKNOWLEDGMENTS

The researchers would like to acknowledge the Water Technology Initiative (WTI) program project no. (EWHF/2019/222) and Department of Science and Technology (DST), New Delhi under INSPIRE faculty award-2018 (MS-146), India, for providing the financial support for this research work.

AUTHOR CONTRIBUTIONS

A.S. planned and synthesized binary nanocomposite and performed experiments and analyzed the data and wrote the manuscript. U.B. performed the electrochemical experiments. D.J. performed the antibacterial activity test for the respective composite. H.S.K. supervised and proofread the manuscript.

DECLARATION OF INTERESTS

The authors declare no competing interests.

Received: March 21, 2022
Revised: May 31, 2022
Accepted: August 6, 2022
Published: September 16, 2022

REFERENCES

Alqahtani, M.Q. (2014). Tooth-bleaching procedures and their controversial effects: a literature review. Saudi Dent. J. *26*, 33–46. https://doi.org/10.1016/j.sdentj.2014.02.002.

Carey, C.M. (2014). Tooth whitening: what we now know. J. Evid. Based. Dent. Pract. *14*, 70–76. https://doi.org/10.1016/j.jebdp.2014.02.006.

Chen, Y., Deng, X., Wen, J., Zhu, J., and Bian, Z. (2019). Piezo-promoted the generation of reactive oxygen species and the photodegradation of organic pollutants. Appl. Catal. B Environ. *258*, 118024. https://doi.org/10.1016/j.apcatb.2019.118024.

Claros, M., Setka, M., Jimenez, Y.P., and Vallejos, S. (2020). Aacvd synthesis and characterization of iron and copper oxides modified zno structured films. Nanomaterials *10*, 4711–E516. https://doi.org/10.3390/nano10030471.

Colares, V.L.P., Lima, S.N.L., Sousa, N.C.F., Araújo, M.C., Pereira, D.M.S., Mendes, S.J.F., Teixeira, S.A., Monteiro, C.d.A., Bandeca, M.C., Siqueira, W.L., et al. (2019). Hydrogen peroxide-based products alter inflammatory and tissue damage-related proteins in the gingival crevicular fluid of healthy volunteers: a randomized trial. Sci. Rep. *9*, 3457–3511. https://doi.org/10.1038/s41598-019-40006-w.

Dewhirst, F.E., Chen, T., Izard, J., Paster, B.J., Tanner, A.C.R., Yu, W.H., Lakshmanan, A., and Wade, W.G. (2010). The human oral microbiome. J. Bacteriol. *192*, 5002–5017. https://doi.org/10.1128/JB.00542-10.

Fernandes, D., Raubach, C.W., Jardim, P.L., Moreira, M.L., and Cava, S.S. (2021). Synthesis of $NaNbO_3$ nanowires and their photocatalytic activity. Ceram. Int. *47*, 10185–10188. https://doi.org/10.1016/j.ceramint.2020.12.070.

Huan, Y., Wang, X., Hao, W., and Li, L. (2015). Enhanced photocatalysis activity of ferroelectric KNbO3 nanofibers compared with antiferroelectric $NaNbO_3$ nanofibers synthesized by electrospinning. RSC Adv. *5*, 72410–72415. https://doi.org/10.1039/c5ra13680f.

Ji, S., Liu, H., Sang, Y., Liu, W., Yu, G., and Leng, Y. (2014). Synthesis, structure, and piezoelectric properties of ferroelectric and antiferroelectric $NaNbO_3$ nanostructures. CrystEngComm *16*, 7598–7604. https://doi.org/10.1039/c4ce01116c.

Jiang, S., Lin, K., and Cai, M. (2020). ZnO nanomaterials: current advancements in antibacterial mechanisms and applications. Front. Chem. *8*, 580–585. https://doi.org/10.3389/fchem.2020.00580.

Johar, M.A., Afzal, R.A., Alazba, A.A., and Manzoor, U. (2015). Photocatalysis and bandgap engineering using ZnO nanocomposites. Adv. Mater. Sci. Eng. 1–22. https://doi.org/10.1155/2015/934587.

Jung, R.E., Zembic, A., Pjetursson, B.E., Zwahlen, M., and Thoma, D.S. (2012). Systematic review of the survival rate and the incidence of biological, technical, and aesthetic complications of single crowns on implants reported in longitudinal studies with a mean follow-up of 5 years. Clin. Oral. Implants. Res. *23*, 2–21. https://doi.org/10.1111/j.1600-0501.2012.02547.x.

Kawamoto, K., and Tsujimoto, Y. (2004). Effects of the hydroxyl radical and hydrogen peroxide on tooth bleaching. J. Endod. *30*, 45–50. https://doi.org/10.1097/00004770-200401000-00010.

Kimyai, S., Bahari, M., Naser-Alavi, F., and Behboodi, S. (2017). Effect of two different tooth bleaching techniques on microhardness of giomer. J. Clin. Exp. Dent. *9*, e249–e253. https://doi.org/10.4317/jced.53290.

Kumar, D., and Khare, N. (2017). Synthesis of $NaNbO_3$ nanorods as a photoanode material for photoelectrochemical water splitting. Springer Proc. Phys. *178*, 107–109. https://doi.org/10.1007/978-3-319-29096-6_13.

Kumar, D., Sharma, S., and Khare, N. (2021). Piezo-phototronic and plasmonic effect coupled Ag-$NaNbO_3$ nanocomposite for enhanced photocatalytic and photoelectrochemical water splitting activity. Renew. Energy *163*, 1569–1579. https://doi.org/10.1016/j.renene.2020.09.132.

Kwon, S.R., and Wertz, P.W. (2015). Review of the mechanism of tooth whitening. J. Esthet. Restor. Dent. *27*, 240–257. https://doi.org/10.1111/jerd.12152.

Lamont, R.J., and Egland, P.G. (2014). Dental caries. Mol. Med. Microbiol. 945–955. https://doi.org/10.1016/B978-0-12-397169-2.00052-4.

Lamont, R.J., Koo, H., and Hajishengallis, G. (2018). The oral microbiota: dynamic communities and host interactions. Nat. Rev. Microbiol. *16*, 745–759. https://doi.org/10.1038/s41579-018-0089-x.

Lee, Y., Cui, M., Choi, J., Kim, J., Son, Y., and Khim, J. (2018). Degradation of polychlorinated dibenzo-p-dioxins and dibenzofurans in real-field soil by an integrated visible-light photocatalysis and solvent migration system with p-n heterojunction BiVO4/Bi2O3. J. Hazard. Mater. *344*, 1116–1125. https://doi.org/10.1016/j.jhazmat.2017.12.002.

Lei, H., Zhang, H., Zou, Y., Dong, X., Jia, Y., and Wang, F. (2019). Synergetic photocatalysis/piezocatalysis of bismuth oxybromide for degradation of organic pollutants. J. Alloys Compd. *809*, 151840. https://doi.org/10.1016/j.jallcom.2019.151840.

Li, C., Ahmed, T., Ma, M., Edvinsson, T., and Zhu, J. (2013). A facile approach to ZnO/CdS nanoarrays and their photocatalytic and photoelectrochemical properties. Appl. Catal. B Environ. *138–139*, 175–183. https://doi.org/10.1016/j.apcatb.2013.02.042.

Li, X., Chen, X., Yi, Z., Zhou, Z., Tang, Y., and Yi, Y. (2019). Fabriction of ZnO nanorods with strong UV absorption and different hydrophobicity on foamed nickel under different hydrothermal conditions. Micromachines *10*, E164. https://doi.org/10.3390/mi10030164.

Li, Z., Xiong, Y., and Xie, Y. (2003). Selected-control synthesis of ZnO nanowires and nanorods via a PEG-assisted route. Inorg. Chem. *42*, 8105–8109. https://doi.org/10.1021/ic034029q.

Ling, J., Wang, K., Wang, Z., Huang, H., and Zhang, G. (2020). Enhanced piezoelectric-induced catalysis of SrTiO3 nanocrystal with well-defined facets under ultrasonic vibration. Ultrason. Sonochem. *61*, 104819. https://doi.org/10.1016/j.ultsonch.2019.104819.

Liu, Y., Shen, S., Zhang, J., Zhong, W., and Huang, X. (2019). Cu 2−x Se/CdS composite photocatalyst with enhanced visible light photocatalysis activity. Appl. Surf. Sci. *478*, 762–769. https://doi.org/10.1016/j.apsusc.2019.02.010.

Ma, J., Ren, J., Jia, Y., Wu, Z., Chen, L., Haugen, N.O., Huang, H., and Liu, Y. (2019). High efficiency bi-harvesting light/vibration energy using piezoelectric zinc oxide nanorods for dye decomposition. Nano Energy *62*, 376–383. https://doi.org/10.1016/j.nanoen.2019.05.058.

Markovic, L., Jordan, R.A., Lakota, N., and Gaengler, P. (2007). Micromorphology of enamel surface after vital tooth bleaching. J. Endod. *33*, 607–610. https://doi.org/10.1016/j.joen.2007.01.011.

Mohd Adnan, M.A., Julkapli, N.M., and Abd Hamid, S.B. (2016). Review on ZnO hybrid photocatalyst: impact on photocatalytic activities of water pollutant degradation. Rev. Inorg. Chem. *36*, 77–104. https://doi.org/10.1515/revic-2015-0015.

Molak, A., Paweczyk, M., Kubacki, J., and Szot, K. (2009). Nano-scale chemical and structural segregation induced in surface layer of $NaNbO_3$ crystals with thermal treatment at oxidising conditions studied by XPS, AFM, XRD, and electric properties tests. Phase Transitions *82*, 662–682. https://doi.org/10.1080/01411590903341155.

Ngo-Duc, T., Singh, K., Meyyappan, M., and Oye, M.M. (2012). Vertical ZnO nanowire growth on metal substrates. Nanotechnology *23*, 194015. https://doi.org/10.1088/0957-4484/23/19/194015.

Pan, C., Dong, L., Zhu, G., Niu, S., Yu, R., Yang, Q., Liu, Y., and Wang, Z.L. (2013). High-resolution electroluminescent imaging of pressure distribution using a piezoelectric nanowire LED array. Nat. Photonics *7*, 752–758. https://doi.org/10.1038/nphoton.2013.191.

Perelshtein, I., Applerot, G., Perkas, N., Wehrschetz-Sigl, E., Hasmann, A., Guebitz, G.M., and Gedanken, A. (2009). Antibacterial properties of an in situ generated and simultaneously deposited nanocrystalline ZnO on fabrics. ACS Appl. Mater. Interfaces *1*, 361–366. https://doi.org/10.1021/am8000743.

Román-Rodríguez, J.L., Agustín-Panadero, R., Roig-Vanaclocha, A., and Amengual, J. (2020). A tooth whitening and chemical abrasive protocol for the treatment of developmental enamel defects. J. Prosthet. Dent. *123*, 379–383. https://doi.org/10.1016/j.prosdent.2019.02.015.

Saha, M., Ghosh, S., Paul, S., Dalal, B., and De, S.K. (2018). Nb-Dopant-Induced tuning of optical and electrical property of anatase TiO2 nanocrystals. ChemistrySelect *3*, 6654–6664. https://doi.org/10.1002/slct.201800434.

Šćepanović, M., Grujić-Brojčin, M., Vojisavljević, K., Bernik, S., and Srećković, T. (2010). Raman study of structural disorder in ZnO nanopowders. J. Raman Spectrosc. *41*, 914–921. https://doi.org/10.1002/jrs.2546.

Sharma, A., Bhardwaj, U., and Kushwaha, H.S. (2021a). Materials Advances Using Ultrasonic Vibrations. https://doi.org/10.1039/d1ma00106j.

Sharma, A., Bhardwaj, U., and Kushwaha, H.S. (2021b). Ba2TiMnO6two-dimensional nanosheets for rhodamine B organic contaminant degradation using ultrasonic vibrations. Mater. Adv. *2*, 2649–2657. https://doi.org/10.1039/d1ma00106j.

Sharma, A., Bhardwaj, U., and Kushwaha, H.S. (2021c). Efficacious visible-light photocatalytic degradation of toxics by using Sr2TiMnO6-rGO composite for the wastewater treatment. Clean. Eng. Technol. *2*, 100087. https://doi.org/10.1016/j.clet.2021.100087.

Sharma, A., Bhardwaj, U., and Kushwaha, H.S. (2022). ZnO hollow pitchfork: coupled photo-piezocatalytic mechanism for antibiotic and pesticide elimination. Catal. Sci. Technol. *12*, 812–822. https://doi.org/10.1039/d1cy01973b.

Shen, Z.X., Wang, X.B., Kuok, M.H., and Tang, S.H. (1998). Raman scattering investigations of the antiferroelectric–ferroelectric phase transition of $NaNbO_3$. J. Raman Spectrosc. *29*, 379–384. https://doi.org/10.1002/(sici)1097-4555(199805)29:5<379::aid-jrs249>3.3.co;2-6.

Singh, S., and Khare, N. (2017). Coupling of piezoelectric, semiconducting and photoexcitation properties in $NaNbO_3$ nanostructures for controlling electrical transport: realizing an efficient piezo-photoanode and piezo-photocatalyst. Nano Energy *38*, 335–341. https://doi.org/10.1016/j.nanoen.2017.05.029.

Soeteman, G.D., Valkenburg, C., Van der Weijden, G.A., Van Loveren, C., Bakker, E.W.P., and Slot, D.E. (2018). Whitening dentifrice and tooth surface discoloration—a systematic review and meta-analysis. Int. J. Dent. Hyg. *16*, 24–35. https://doi.org/10.1111/idh.12289.

Tredwin, C.J., Naik, S., Lewis, N.J., and Scully, C. (2006). Hydrogen peroxide tooth-whitening (bleaching) products: review of adverse effects and safety issues. Braz. Dent. J. *200*, 371–376. https://doi.org/10.1038/sj.bdj.4813423.

Wang, H., Chen, T., Chen, D., Zou, X., Li, M., Huang, F., Sun, F., Wang, C., Shu, D., and Liu, H. (2020a). Sulfurized oolitic hematite as a heterogeneous Fenton-like catalyst for tetracycline antibiotic degradation. Appl. Catal. B Environ. *260*, 118203. https://doi.org/10.1016/j.apcatb.2019.118203.

Wang, H., Liu, X., Wang, S., and Li, L. (2018). Dual templating fabrication of hierarchical porous three-dimensional ZnO/carbon nanocomposites for enhanced photocatalytic and photoelectrochemical activity. Appl. Catal. B Environ. *222*, 209–218. https://doi.org/10.1016/j.apcatb.2017.10.012.

Wang, J., and Gao, L. (2004). Hydrothermal synthesis and photoluminescence properties of zno nanowires. Solid State Commun. *132*, 269–271. https://doi.org/10.1016/j.ssc.2004.07.052.

Wang, Y., Wen, X., Jia, Y., Huang, M., Wang, F., Zhang, X., Bai, Y., Yuan, G., and Wang, Y. (2020b). Piezo-catalysis for nondestructive tooth whitening. Nat. Commun. *11*, 1328. https://doi.org/10.1038/s41467-020-15015-3.

Wang, Z., Li, Y., Chen, B., Viswan, R., Li, J.F., and Viehland, D. (2012). Self-assembled $NaNbO_3$-Nb2O5 (ferroelectric-semiconductor) hetero-structures grown on LaAlO3 substrates. Appl. Phys. Lett. *101*, 132902–132904. https://doi.org/10.1063/1.4754713.

Wong, K.A., Lam, S.M., and Sin, J.C. (2019). Wet chemically synthesized ZnO structures for photodegradation of pre-treated palm oil mill effluent and antibacterial activity. Ceram. Int. *45*, 1868–1880. https://doi.org/10.1016/j.ceramint.2018.10.078.

Wongpraparatana, I., Matangkasombut, O., Thanyasrisung, P., and Panich, M. (2018). Effect of vital tooth bleaching on surface roughness and streptococcal biofilm formation on direct tooth-colored restorative materials. Oper. Dent. *43*, 51–59. https://doi.org/10.2341/16-366-L.

Xu, H., Liu, C., Li, H., Xu, Y., Xia, J., Yin, S., Liu, L., and Wu, X. (2011). Synthesis, characterization and photocatalytic activity of NaNbO 3/ZnO heterojunction photocatalysts. J. Alloys Compd. *509*, 9157–9163. https://doi.org/10.1016/j.jallcom.2011.06.100.

Xue, X., Zang, W., Deng, P., Wang, Q., Xing, L., Zhang, Y., and Wang, Z.L. (2015). Piezo-potential enhanced photocatalytic degradation of organic dye using ZnO nanowires. Nano Energy *13*, 414–422. https://doi.org/10.1016/j.nanoen.2015.02.029.

You, H., Ma, X., Wu, Z., Fei, L., Chen, X., Yang, J., Liu, Y., Jia, Y., Li, H., Wang, F., and Huang, H. (2018). Piezoelectrically/pyroelectrically-driven vibration/cold-hot energy harvesting for mechano-/pyro- bi-catalytic dye decomposition of $NaNbO_3$ nanofibers. Nano Energy *52*, 351–359. https://doi.org/10.1016/j.nanoen.2018.08.004.

Zhang, F., Wu, C., Zhou, Z., Wang, J., Bao, W., Dong, L., Zhang, Z., Ye, J., Liao, L., and Wang, X. (2018). Blue-light -activated nano-TiO2@PDA for highly effective and nondestructive tooth whitening. ACS Biomater. Sci. Eng. *4*, 3072–3077. https://doi.org/10.1021/acsbiomaterials.8b00548.

Zhang, H., Zhu, Y., Li, Y., Qi, X., Yang, J., Qi, H., Li, Q., Ma, Y., Zhang, Y., Zhang, X., and Zhang, L. (2021). A bifunctional zwitterion-modified porphyrin for photodynamic nondestructive tooth whitening and biofilm eradication. Adv. Funct. Mater. *31*, 2104799. https://doi.org/10.1002/adfm.202104799.

Zhang, L.Y., Fang, Z.H., Li, Q.L., and Cao, C.Y. (2019). A tooth-binding antimicrobial peptide to prevent the formation of dental biofilm. J. Mater. Sci. Mater. Med. *30*, 45. https://doi.org/10.1007/s10856-019-6246-6.

STAR★METHODS

KEY RESOURCES TABLE

REAGENT or RESOURCES	SOURCE	IDENTIFIER
Chemicals, Peptides, and Recombinant Proteins		
$Zn(NO_3)_2.6H_2O$	Loba Chemie	CAS no-10196-18-6
$(NH_4)_2CO_3$	Loba Chemie	CAS no- 506-87-6
Nb_2O_5	SRL	CAS no-1313-96-8
Polyethylene Glycol (Molecular Weight 300)	Merck	CAS no- 25,322-68-3
Rhodamine B	Loba Chemie	CAS no- 81-88-9
Rose Bengal	Sigma Aldrich	CAS no- 632-69-9
Methylene Blue	Sigma Aldrich	CAS no- 28,983-56-4
Others		
ZnO	JCPDS	JCPDS no- 36-1451
$NaNbO_3$	JCPDS	JCPDS no- 01-082-0606

RESOURCE AVAILABILITY

Lead contact

Further information and requests for resources should be directed to and will be fulfilled by the lead contact, Dr. Himmat Singh Kushwaha (himmatsingh.mrc@mnit.ac.in).

Materials availability

All materials generated in this study are available from the lead contact without restriction.

Data and code availability

This paper does not report original code.

Any additional information required to reanalyze the data reported in this paper is available from the lead contact upon request.

METHOD DETAILS

Synthesis of $NaNbO_3$-ZnO binary nanocomposite

The hydrothermal technique was used to produce $NaNbO_3$/ZnO binay nanocomposite. It is a two-step process. In step one: 1M of $Zn(NO_3)_2.6H_2O$ and 1M of $(NH_4)_2CO_3$ were vigorously combined to produce white precipitate. This white precipitate was then filtered and washed multiple times with deionized water to remove unwanted residues. After washing, this whitish residue was dispersed in a solution of 0.4% Polyethylene glycol (PEG, molecular weight: 300) (Li et al., 2003; Wang and Gao, 2004). In step two: 0.4 g of Nb_2O_5 were dissolved in 20M sodium hydroxide (NaOH), this solution was then added in the above solution which was prepared in step one. The resulting solution was put into a 100 mL of stainless-steel autoclave lined with Teflon, and maintained at 200 °C for 10 h (Fernandes et al., 2021; You et al., 2018). The precipitate that formed was handled in the same manner as described previously and dried in a vacuum oven for 6 h at 60 °C.

Piezocatalytic activity experiments

The piezocatalytic behavior of $NaNbO_3$/ZnO was evaluated by using the degradation of three different organic dyes of 10 mg/L -Rhodamine B, Methylene Blue, and Rose Bengal by utilizing an ultrasonic cleaner to create mechanical stress (Ling et al., 2020). In a separate glass beaker, 40 mL of each dye solution was collected. To obtain the adsorption-desorption equilibrium between the dye molecules and the $NaNbO_3$/ZnO binary nanocomposite (Lei et al., 2019), 1mg per mL catalyst was placed in a glass beaker proceeded by 30 min of continuous stirring in dark. During the degradation process, at certain time

intervals 2 mL of the solution was collected and centrifuged. The concentration of these organic dyes was determined by analyzing absorbance values using the UV-Visible spectrophotometer. After that, the entire glass beakers were placed in an ultrasonic water bath (120W, 40 kHz). Throughout this experiment, ultrasonic water was regularly changed with cold water to maintain it at room temperature (Sharma et al., 2021a).

Electrochemical measurements

The electrochemical investigation of $NaNbO_3$/ZnO binary nanocomposite were performed by using a standard three-electrode electrochemical workstation (Biologic EC lab sp-150). A platinum wire was act as a counter electrode; the reference electrode was Ag/AgCl, and the working electrode was $NaNbO_3$/ZnO binary nanocomposite, while the electrolyte being 0.1 M KOH solution. Working electrode was initially prepared by the ink formation. For the ink formation, 20 mg of catalyst was added in 1 mL of IPA (isopropanol alcohol) and then 20 μL of Nafion was added to the mixture as a binder. This mixture was kept in an ultrasonic bath for 2 h.

Scavenger experiment

This study was carried out to determine the active component involved for the degradation of organic contaminants by piezocatalytic activity of the $NaNbO_3$/ZnO binary nanocomposite. Isopropanol alcohol (IPA) scavenged hydroxyl radicals (OH·), Na-ethylenediaminetetraacetate (EDTA) scavenged holes (h^+), and *para*-benzoquinone (BQ) scavenged superoxide ($\cdot O_2^-$). All these scavengers (1 mM) were combined with the $NaNbO_3$/ZnO and Rh. B solution in a different beaker, and these beakers were kept for the piezocatalysis.

Piezo-potential measurement

The piezo potential measurement for $NaNbO_3$/ZnO binary nanocomposite was perform on Digital Scanning Oscilloscope (DSO). Initially, $NaNbO_3$/ZnO binary nanocomposite pallet was formed. After the pallet formation, contacts have been made on one side and the other side was insulated. The pallet was connected to the DSO and was put in the ultrasound system. When the ultrasound system was ON, the increased potential was seen on the DSO screen.

Tooth cleaning experiment

The extracted human teeth were submerged in a combination of coffee, black tea, cold drink, and tobacco for 1week prior to the tooth brightening procedure. After drenching, the teeth were rinsed with distilled water to eliminate any residual staining substances on the surface. Rinsing continued until the drain water was clean. After that, Kim wipes was used to dry the teeth. The pigmented teeth were put in separate beakers containing 40 mL of distilled water, 40 mL of $NaNbO_3$/ZnO suspension (1 mg/mL). After 30 min of stirring, the beakers were then placed in an ultrasonic water bath and vibrated for 6 h. Figure S1 shows an experimental setup of the tooth cleaning experiment. In the given figure, the tooth was hooked by a clamp, and it was cleaned with $NaNbO_3$/ZnO binary nanocomposite aqueous solution by using an electric toothbrush.

Antibacterial activity tests

The antibacterial activities of $NaNbO_3$/ZnO binary nanocomposite were assessed as zone of inhibition using agar well diffusion method against *E. coli* ATCC 25922. Briefly, 1 mL overnight grown *E. coli* suspension ($>10^7$ CFU mL^{-1}) was spread onto the surface of LB agar Petri-plates and then wells were punctured on LB agar Petri-plates using sterile cork-borer. Afterward, 100 μL of $NaNbO_3$/ZnO binary nanocomposite (1g L^{-1}) were loaded into each well and incubated overnight at 37 °C for the development of the zone of inhibition (Wong et al., 2019). The measurement of zone of inhibition was performed by measuring the mean diameter around the $NaNbO_3$/ZnO binary nanocomposite in mm.

In another experiment, 1 mL of overnight grown culture was inoculated in 10 mL fresh LB medium and incubated at 37 °C for 4 h to optimize the *E. coli* growth condition. Subsequently, 1 g L^{-1} $NaNbO_3$/ZnO binary nanocomposite was added into the medium and then vortexed for piezocatalytic inactivation of the bacteria. Further the samples were allowed incubated in an incubator shaker at 37 °C at 200 rpm constant shaking to ensure maximum contact between $NaNbO_3$/ZnO binary nanocomposite and *E. coli* and from test *E. coli* solutions, 500 μL was pipette at 0, 15, 30, 45 and 60 min time intervals and spread onto the

LB agar plates and incubated at 37 °C for 24 h for the formation of bacterial colonies. All the experiments were performed in triplicate to avoid any experimental errors.

Materials characterizations

X-ray Diffractometer analysis was done by using X Pert Pro Panalytical with Cu Kα radiation (2θ = 30-80°, λ = 1.5406 Å). Raman Spectroscopy was performed using IRIX STR 500 Raman spectrometer. The measurements were taken at 25 °C with a 532 nm Ar ion laser (about 1 mW, 50 objective). Scanning electron microscopy pictures were obtained by using Nova Nano FE-SEM 450-FEI. The X-ray photoelectron spectroscopy (XPS) analysis of the synthesized binary nanocomposite was performed using Omicron ESCA + XPS. The optical characteristics of the material were investigated using a dual beam UV-Vis NIR Spectrophotometer (LAMBDA 750-Perkin Elmer). The generation of hydroxyl radicals (OH·) was measured using a fluorescence spectrometer (LS 55 (Perkin Elmer)) in the excitation range 200-800 nm. To identify the piezo response of $NaNbO_3$/ZnO binary nanocomposite piezoresponsive force microscopy (PFM, Bruker Dimension icon scanasyst) was used. A digital scanning oscilloscope (DSO) was used to measure the piezoelectric voltage production under stress. A biologic workstation was used to analyze transient piezo current response and electrochemical impedance spectroscopy (EIS).